ORIGINAL PAPER

Theoretical Study on the Growth Behavior and Photoelectron Spectroscopy of Lanthanum-Doped Silicon Clusters LaSi$_n^{0/-}$ (n = 6–20)

Yaqing Chen[1] · Yuming Liu[2] · Suying Li[1] · Jucai Yang[1,2]

Abstract

The growth behavior and electronic properties of the lowest energy structures of neutral LaSi$_n$ (n = 6–20) and their anions were explored by means of the ABCluster global structure searching strategy combined with the mPW2PLYP double-hybrid density functional. The results revealed that the growth behavior of the lowest energy structures of anionic LaSi$_n^-$ (n = 10–20) clusters choose La-linked two silicon subclusters to La-encapsulated in silicon cages. For neutral LaSi$_n$ (n = 6–20), the growth behavior of the lowest energy structures from substitutional structure to linked motifs and finally to encapsulated configurations occurs at n = 14 and 20, respectively. The simulated photoelectron spectroscopy, adiabatic electron affinities, vertical detachment energies, relative stability and HOMO–LUMO energy gaps were presented. Analyses of HOMO–LUMO energy gaps, relative stability, and chemical bonding reveal that the LaSi$_{20}^-$ possesses ideal thermodynamic and chemical stability in a high I_h-symmetry endohedral motif, which can turn it into suitable constitutional units for cluster-assembled nanomaterials.

Keywords The lowest energy structure of La-doped Si clusters · Structural growth behavior · Simulated photoelectron spectroscopy · Relative stability · mPW2PLYP

Introduction

Study of equilibrium geometries, electronic structures and properties of atomic clusters, especially silicon based on semiconductor clusters, has been an extraordinarily active area of research in the last few decades because of its importance nanoscience and nanotechnology [1–15]. Theoretical modeling and experimental probing of silicon nanoclusters with modified new geometries show possibility of using them as nano-devices in opto-electronics,

tunable lasers, etc. Especially, rare-earth modified silicon-based nanomaterals as "industrial vitamins" have been widely used in various fields such as metallurgy, military, petrochemical, glass ceramics, and new materials owing to their novel magnetic, optical and electrical properties and chemical stability [16–29]. The functional properties with a combination of good flexural strength, fracture toughness, hardness and low Schottky barrier heights make lanthanum modified silicon-based nanomaterials are ideal in devices such as substrates of the integrated circuits, host lattices for light emitting phosphors, ohmic contacts and rectifying contacts [30, 31]. The unique structures and properties of nanoclusters make they are one of the central issues in nanomaterials sciences. Therefore, it is very significant to probe the evolution of lanthanum-silicon aggregates in the transition from the molecular to condensed phase.

Only growth behavior of neutral LaSi$_n$ clusters with n up to 21 has been studied by single-hybrid density functional and concluded that La atom prefers locating on the surface site of the clusters in the size range of n ≤ 10 or n ≤ 12, surrounded by Si atom with basketlike structures with 11 ≤ n ≤ 15, and completely encapsulated into fullerene cage geometries with 16 ≤ n ≤ 21 [32–34]. It is well

✉ Jucai Yang
yangjc@imut.edu.cn

1 School of Energy and Power Engineering, Inner Mongolia University of Technology, Hohhot 010051, People's Republic of China

2 School of Chemical Engineering, Inner Mongolia University of Technology and Inner Mongolia Key Laboratory of Theoretical and Computational Chemistry Simulation, Hohhot 010051, People's Republic of China

known that the functional dependence on the predicted lowest-energy structure always occur for small- or medium-clusters, especially for clusters including rare earth- or transition- metal atoms. So the calculation method adopted is quite important. In light of our experience [35–40], performances of prediction structures and properties of double-hybrid density functional are better than those of pure or single-hybrid density functional for rare earth-metal atom doped silicon clusters. In this paper, the ABCluster global search technique combined with a double-hybrid density functional scheme was adopted to optimize geometries of La-doped $Si_n^{0/-}$ ($n = 6$–20) clusters with the goal of illuminating the growth behavior of the ground states, exploring the electronic properties, knowing the bonding characteristics, and furnishing important information for further studies of introducing other transition or rare-earth metals into semiconductor nanoclusters. We will see that the growth behavior of the ground states predicted in this paper is different from those reported previously [32–34].

Computational Details

Three techniques were adopted to search the initial geometries for $LaSi_n^{0/-}$ ($n = 6$–20) clusters. First, using the ABCluster global search technique [41] coupled with PBE functional [42] and with the 6-31G basis set for Si atoms and ECP46MWB basis set [43, 44] for La atoms, more than 300 geometries for each cluster were optimized. The detailed description of ABCluster global search technique is elsewhere [36, 38, 39]. Second, the substitutional structure schemes were adopted, in which a Si atom in the most stable structure of Si_{n+1} was replaced with a La atom. Third, geometries already presented in the preceding publications [20, 24] were adopted. The obtained low-lying candidate structures of the global minimum for each size were reoptimized using PBE functional in collaboration with the Stuttgart/Dresden ECPs (i.e., SDD) basis set [44, 45] for La atoms and all-electron cc-pVTZ basis set [46] for Si atoms. The vibrational frequency calculations were carried out at the same level to assure the nature of the stationary points. After accomplishment of the initial structure optimization using PBE, the low-lying isomers are again selected and reoptimiezed by means of a double hybrid mPW2PLYP functional [47] with the same basis sets. Vibrational frequency was not carried out at the mPW2PLYP level. In order to farther refine the energies, calculations of single-point energy were carried out at the mPW2PLYP level with aug-cc-pVTZ basis set [46] for Si atoms (basis set for La atoms unchanged). According to Koopmans' theorem [48, 49], we simulated the photoelectron spectroscopy (PES) of anionic species at the mPW2PLYP level with the Multiwfn program [50]. To further understand the interaction between La atom and silicon clusters, the chemical bonding analyses in light of AdNDP (adaptive natural density partitioning) [51] were also performed. All of the calculations were implemented using the Gaussian 09 package [52].

To examine the relativistic effects and the reliability of the methods used in this work, single-point energy calculations were also executed by means of the ROCCSD(T) scheme with the aug-cc-pVTZ-DK basis set [46] for Si atoms and cc-pVTZ-DK3 basis set [53] for La atoms and the Douglas-Kroll-Hess scalar relativistic correction [54–56] for $LaSi_n^{0/-}$ ($n = 1$–5) small clusters. The ground-state structure and several low-lying isomers of $LaSi_n^{0/-}$ ($n = 1$–5) together with their point ground, electronic state, and relatively energies are exhibited in Figure S1 in Supplementary Information. The adiabatic electron affinity (AEA) and the vertical detachment energy (VDE) of $LaSi_n^{0/-}$ ($n = 1$–5) are also listed in Table S1 in Supplementary Information. From Figure S1 we can see that the ground state structure and energetic order of isomers evaluated by the mPW2PLYP and ROCCSD(T) schemes are identical. From Table S1 we can see that the AEAs and VDEs calculated by the mPW2PLPY scheme are in good agreement with the results predicted by the ROCCSD(T) scheme. The mean absolute deviations of mPW2PLYP result from ROCCSD(T) data are by 0.10 eV. The largest deviation is that of $LaSi_3^-$, which is off by 0.29 eV for AEA and 0.19 eV for VDE. If $LaSi_3^-$ is removed, the mean absolute deviation is only 0.07 eV. All of these indicate that the results of mPW2PLYP are reliable.

Results and Discussion

The Lowest Energy Structures

The lowest energy geometries of $LaSi_n$ ($n = 6$–20) clusters and their anions are exhibited in Figs. 1 and 2, respectively. The electronic state, average binding energies, HOMO–LUMO energy gap, and NPA charges on the La atom for the lowest energy structure are scheduled in Table 1. The corresponding low-lying structures, point ground and relative energies are exhibited in Figures S2 and S3 in Supplementary Information. For negatively charge ions, the predicted spin states of $LaSi_n^-$ ($1 \leq n \leq 20$) are single excluded $LaSi^-$ and $LaSi_2^-$ which is triplet as can be seen in Figure S1. For neutral clusters, the evaluated spin states are double.

The growth behavior of the lowest energy structures of anionic lanthanum doped Si clusters choose linked to encapsulated configuration in light of the results of the
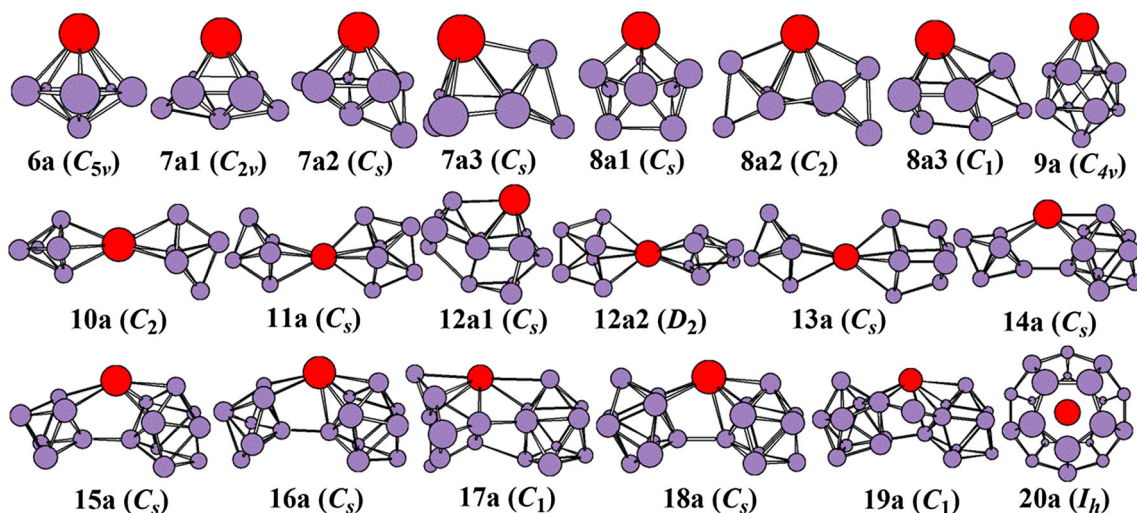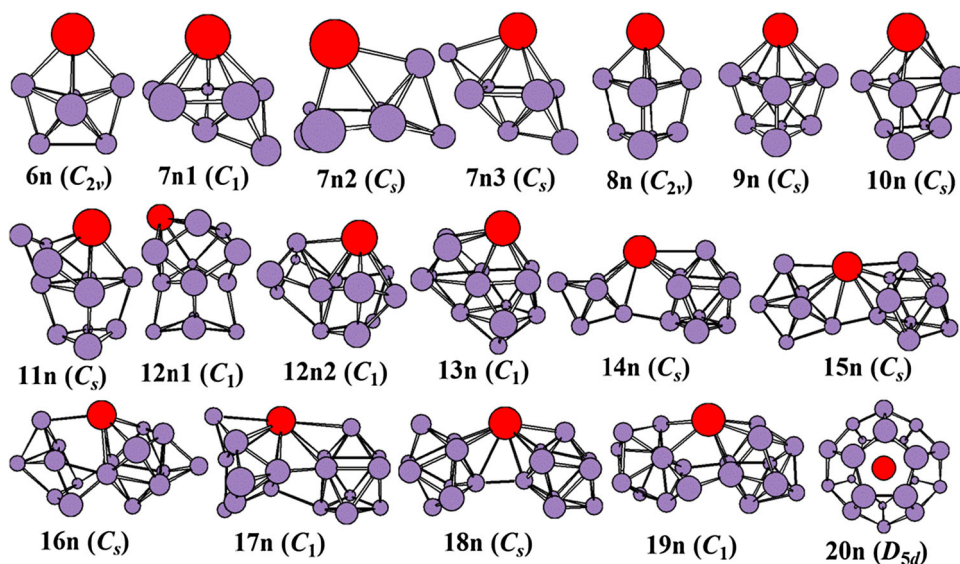
Fig. 1 The lowest energy structures of $LaSi_n^-$ ($n = 6$–20) and their point group

Fig. 2 The lowest energy structures of $LaSi_n$ ($n = 6$–20) and their point group

double-hybrid mPW2PLYP scheme. For n = 6, the lowest energy structure is a pentagonal bipyramid with La atom located on the quintuple axis. For n = 7, three topological isomers (**7a1**, **7a2** and **7a3**) compete with each other for the lowest energy structure due to the fact that their energy is nearly degenerate. Their maximum energy differences are only 0.03 eV (see Figures S2). For n = 8, the situation is similar to n = 7, three geometries (**8a1**, **8a2** and **8a3**) are also compete with each other for the lowest energy structure. In fact the **8a1**, **8a2** and **8a3** isomers can be regarded as attaching a Si atom to the **7a1**, **7a2** and **7a3** geometries, respectively. The **8a2** structure is linked configuration in which La atom links to two tetrahedron Si_4 subclusters. For n = 9, the lowest energy structure is a C_{4v}-symmetry bi-face-capped tetragonal antiprism. For n = 10–19, the lowest-energy structure is linked configurations. The La atom

in $LaSi_{10}^-$ links two orthogonal trigonal bipyramid Si_5 subclusters, in $LaSi_{11}^-$ connects a trigonal bipyramid Si_5 and a face-capped trigonal bipyramid Si_6, in $LaSi_{13}^-$ connects a trigonal bipyramid Si_5 and a distorted bicapped octahedron Si_8, in $LaSi_{14}^-$ connects a trigonal bipyramid Si_5 and a TTP (tricapped trigonal prism) motif of Si_9, in $LaSi_{15}^-$ connects an octahedron Si_6 and a TTP Si_9, in $LaSi_{16}^-$ links a pentagonal bipyramid Si_7 and a TTP Si_9, in $LaSi_{17}^-$ links a Si_8 subcluster and a TTP Si_9, in $LaSi_{18}^-$ links to two TTP Si_9, in $LaSi_{19}^-$, along with a Si atom, links to two TTP Si_9. For n = 12, both **12a1** and **12a2** isomer compete with each other for the lowest energy structure. The energy difference between **12a1** and **12a2** is only 0.03 eV (see Figures S2). The **12a2** structure is linked configuration in which La atom links to two orthogonal face-capped trigonal bipyramid Si_6 subclusters. The **12a1**

Table 1 Electronic state, average bonding energy E_b (eV), HOMO–LUMO energy gap E_{gap} (eV), and the charge on the La atom Q(La) (a.u.) of the lowest energy structure of $LaSi_n^{0/-}$ ($n = 6$–20) clusters

n	$LaSi_n^-$				$LaSi_n$			
	State	Eb	Egap	Q(La)	State	Eb	Egap	Q(La)
6	$^1A_1$	4.40	3.28	0.24	$^2A_2$	4.31	2.73	0.52
7	$^1A_1$	4.49	3.43	0.07	^1A	4.36	3.82	0.42
8	$^1A'$	4.58	3.24	0.16	$^2A_1$	4.46	2.77	0.51
9	$^1A_1$	4.67	3.19	0.42	$^2A'$	4.53	2.88	0.50
10	^1A	4.66	4.51	0.71	$^2A''$	4.54	3.37	0.48
11	$^1A'$	4.69	4.39	0.42	$^2A'$	4.57	3.40	0.15
12	$^1A'$	4.71	3.44	0.23	^2A	4.59	3.52	0.56
13	$^1A'$	4.72	4.34	0.34	^2A	4.62	3.50	0.43
14	$^1A'$	4.76	3.85	0.22	$^2A'$	4.64	4.20	0.47
15	$^1A'$	4.76	3.81	0.24	$^2A'$	4.64	3.81	0.15
16	$^1A'$	4.76	3.72	0.32	$^2A'$	4.65	3.17	0.25
17	^1A	4.76	3.80	0.19	^2A	4.65	4.10	0.31
18	$^1A'$	4.79	2.76	0.17	$^2A'$	4.68	3.33	0.33
19	^1A	4.79	3.71	0.42	^2A	4.68	3.58	0.50
20	^1A_g	4.91	2.42	− 2.55	^2A_u	4.77	2.31	− 2.97

geometry can be viewed as linked configuration in which La atom connects a rhombus Si_4 and a Si_8 subcluster. For $n = 20$, the lowest energy structure is encapsulated configuration with La atom located in the silicon cage.

The growth behavior of the lowest energy structures of neutral $LaSi_n$ ($n = 6$–20) from substitutional geometries to linked structures and finally to encapsulated configurations happens at $n = 14$ and 20, respectively. The lowest energy structure of $LaSi_6$ belongs to substitutional structure in which a La atom was substituted for a horizontal Si atom of the lowest energy pentagonal bipyramidal structure of Si_7 [2–4, 6]. For $n = 7$, similarly to its anion, three topological isomers (**7n1**, **7n2** and **7n3**) compete with each other for the lowest energy structure. The **7n3** is substitutional structure in which a La atom was substituted for a Si atom of the lowest energy Si_8 bicapped octahedron [3, 4, 6]. The energy difference between **7n3** and **7n1** is only 0.03 eV (see Figures S3). Practically the capped Si atom connected the La atom in **7n3** isomer is weakly bound and moves almost freely to the position of **7n1** geometry. The lowest energy structures **8n**, **9n**, **10n**, **11n**, **12n1**, **12n2** and **13n** also belong to substitutional structures, which can be viewed as the lowest energy structure of Si_9, Si_{10}, Si_{11}, Si_{12}, Si_{13} and Si_{14} [3–6], respectively, with a Si atom replaced by a La atom. The lowest energy structures **8n**, **9n**, **10n**, **11n**, **12n1**, and **13n** are different from those of their corresponding anions. The **12n2** geometry, corresponding to anionic **12a1**, belongs to not only linked structure, but also substitutional structure. The energy

difference between **12n1** and **12n2** is only 0.01 eV, indicating the energy of both is degenerate. For $n = 14$–19, the lowest energy structures are linked configurations. And excluded $LaSi_{16}$ they are similar to those of their anions. The La atom in the lowest energy structure of $LaSi_{16}$ links an anomalous Si_7 and an anomalous Si_9 subclusters. Starting from $n = 20$, the lowest energy structure is encapsulated framework with La atom centered in the silicon cage. It is noted that most the lowest energy structures are different from those reported previously [32], for example n = 11–19.

Simulated PES of Anionic Clusters

PES as a powerful can examine the lowest energy structures due to the fact that the PES is susceptible to changes of the structure. Therefore, in light of theoretical generalized Koopman theorem [48, 49], we simulated the PES spectra of the lowest energy structure of the anions at the mPW2PLYP level with the Multiwfn program [50]. First, the relative energy of the orbital (ΔE_n) is computed by the equation during the simulation:

$$\Delta E_n = \Delta E_{HOMO-n} - \Delta E_{HOMO} \tag{1}$$

Second, the first peak associated with the HOMO is set at the VDE position, and the peaks associated with the deeper orbitals are shifted to higher binding energy based on the value of $-\Delta E_n$. Third, the peaks are fitted with a Gaussian function of 0.25 eV full widths at half maximum. The simulated PES is accomplished and shown in Fig. 3. It can be seen from the simulated PES of $LaSi_6^-$ that there are three major peaks located at 2.78, 3.39, and 4.56 eV in the range of ≤ 5.0 eV, respectively. For n = 7, three isomers are simulated. The simulated PES of **7a1** has two double peaks. One is located at 2.74 and 2.94 eV, and another is centered at 4.37 and 4.58 eV. The simulated PES of **7a2** shows four peaks centered at 2.51, 3.22, 3.97 and 4.80 eV, respectively. Six peaks centered at 2.51, 3.13, 3.55, 3.91, 4.15 and 4.56 eV are observed in the simulated PES of **7a3**. For n = 8, three isomers are also simulated. The simulated PES of **8a1** and **8a3** has five peaks, located at 2.76, 3.05, 3.47, 4.29 and 4.64 eV and 2.74, 2.95, 3.24, 3.75 and 4.56 eV, respectively. Six peaks located at 2.91, 3.24, 3.62, 3.99, 4.30 and 4.75 eV are inspected for **8a2**. For n = 9, 11, 14, and 18, they all have three peaks, locating at 3.08, 3.94 and 4.34 eV, 3.71, 4.10 and 4.96 eV, 3.60, 4.07 and 4.63 eV, and 3.65, 4.19 and 4.81 eV, respectively. For n = 10, 13, 16, and 17, they all have two peaks, centering at 3.96 and 4.33 eV, 4.32 and 4.80 eV, 3.97 and 4.36 eV, and 3.36 and 4.14 eV, respectively. For n = 12, two isomers are simulated. There are four peaks for **12a1** located at 3.14, 3.44, 3.82, and 4.27 eV, and two peaks for **12a2** centered at 3.49 and 4.46 eV, respectively.
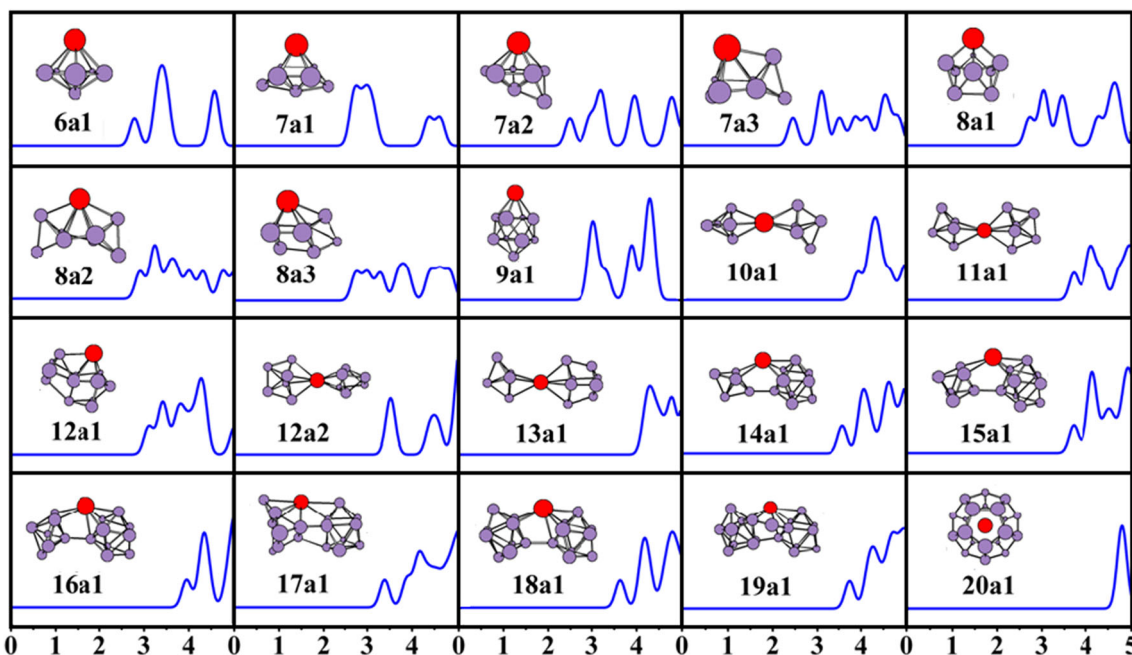
Fig. 3 Simulated PES spectra of the lowest energy $LaSi_n^-$ ($n = 6$–20) clusters

For n = 15 and 19, both have four peaks located at 3.70, 4.12, 4.49 and 4.91 eV, and 3.74, 4.26, 4.72 and 4.94 eV, respectively. Only one peak centered at 4.75 eV is observed for simulated PES of $LaSi_{20}^-$ in the range of ≤ 5.0 eV. We expect that these simulations will give forceful motivation for experimental studies of La-doped silicon clusters and their anions.

Electron affinity is also a key spectral data and extremely significant for use in the chemical reaction process to determine charge transfer, bond dissociation energies and so on. AEA is defined as the energy difference in the manner [35]:

$$AEA = E_{neutral} - E_{anion} + \Delta E_{Sc} \qquad (2)$$

where $E_{neutral}$ and E_{anion} are the lowest energy of the neutral and anionic clusters, respectively. And ΔE_{sc} is an empirical structural correction factor based on the result of $ScSi_n^-$ clusters [35]. The charge of a metal atom in a cluster generally inclines to be positive or slightly negative. However, it will be negatively charged when the numbers of silicon atom increase and the cluster becomes a cage structure. In light of the charge's change, the structures of cluster are categorized into three types: no-cage, half-cage, and cage. The numerical numbers of ΔE_{sc} are assigned to be 0.00, − 0.20 and − 0.40 eV for no-cage, half-cage and cage structures, respectively [35]. The calculated AEAs of $ScSi_n^-$ with structural correction factor are in excellent agreement with the experimental data, and the average absolute error is only 0.08 eV [35]. Therefore, we took the structural correction factor into account when we
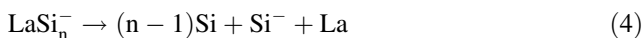
calculated the AEAs of YSi_n^- clusters. The charges on the La atom are positive for n = 6–19 as can be seen from Table 1, while n = 20 are large negatively charged. So the lowest energy structure of $LaSi_n^-$ with n = 6–19 is no-cage, but cage motif with n = 20. Because the radius of La is larger than that of Sc, the La-doped Si clusters do not appear as the half-cage like the Sc-doped Si clusters [35]. Hence, the ΔE_{sc} is 0.00 eV for n = 6–19 and -0.40 eV for n = 20. The theoretical AEA and VDE are listed in Table 2. There are no experimental values for comparison.

Table 2 The theoretical adiabatic electron affinity (AEA) and vertical detachment energy (VDE) for $LaSi_n^-$ (n = 6–20)
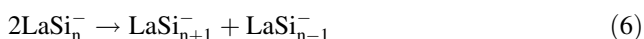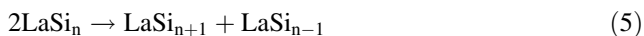
Species	VDE	AEA
6a1	2.78	2.02
7a1	2.74	2.40
8a1	2.76	2.40
9a1	3.08	2.77
10a1	3.96	2.59
11a1	3.71	2.71
12a1	3.14	2.95
13a1	4.32	2.74
14a1	3.60	3.20
15a1	3.70	3.28
16a1	3.97	3.26
17a1	3.36	3.21
18a1	3.65	3.47
19a1	3.74	3.56
20a1	4.75	3.82

Relative Stability

Both atomization energy (AE) and second energy difference (Δ^2E) associated with thermodynamic and relative stability have been calculated for the lowest energy structure of $LaSi_n^{0/-}$ (n = 6–20) clusters. The AE is the energy required for the following reactions:

$$LaSi_n \rightarrow nSi + La \tag{3}$$

$$LaSi_n^- \rightarrow (n-1)Si + Si^- + La \tag{4}$$

The Δ^2E is the energy required the following reactions:

$$2LaSi_n \rightarrow LaSi_{n+1} + LaSi_{n-1} \tag{5}$$

$$2LaSi_n^- \rightarrow LaSi_{n+1}^- + LaSi_{n-1}^- \tag{6}$$

The evaluated AE and Δ^2E are pictured in Fig. 4. It can be seen from Fig. 4a that (1) the AE values of negatively charged ions are all larger than those of their neutrals due to the fact that the $LaSi_n$ is open-shell clusters, while $LaSi_n^-$ is closed-shell clusters. The closed shell configurations minimize the electronic repulsions according to the Pauli exclusion principle. The higher data of the AE, the more stable the clusters. The most stable structure is anionic $LaSi_{20}^-$. (2) The cluster size distributions starting from n = 12 for $LaSi_n^-$ anions and n = 14 for $LaSi_n$ neutral display even–odd alternations. The clusters with an odd numbers of silicon atoms are less stable than those with an even numbers. However, for small clusters, $LaSi_9^-$ is obviously more stable than its adjacent clusters. These consequences are distinctly reproduced in Fig. 4b due to the fact that the Δ^2E are a susceptive measure for relative stability.

To some extent, HOMO–LUMO energy gap (Egap) can be viewed as a significant criterion to reflect the chemical reactivity, especially for a substance containing rare earth elements which sometimes possess novel photochemical sensitivity. The larger the Egap, the weaker the chemical reactivity. The Egap of $LaSi_n^{0/-}$ (n = 6–20) clusters are drawn in Fig. 4c. There are no the odd–even oscillation behavior for Egap. For $LaSi_n^-$, the Egap of n = 10,11 and 13 is relatively large and range from 4.34 to 4.51 eV. For n = 20, the Egap is the smallest, and by 2.42 eV. For neutral $LaSi_n$, the Egap for n = 14 and 17 is relatively large and range from 4.10 to 4.20 eV. The smallest Egap is 2.31 eV of $LaSi_{20}$ cluster. The Egap of anion YSi_{20}^- is very close to that of the corresponding neutral, showing that an extra electron does not change its chemical reactivity, but improves its thermodynamic stability.

Chemical Bonding Analysis

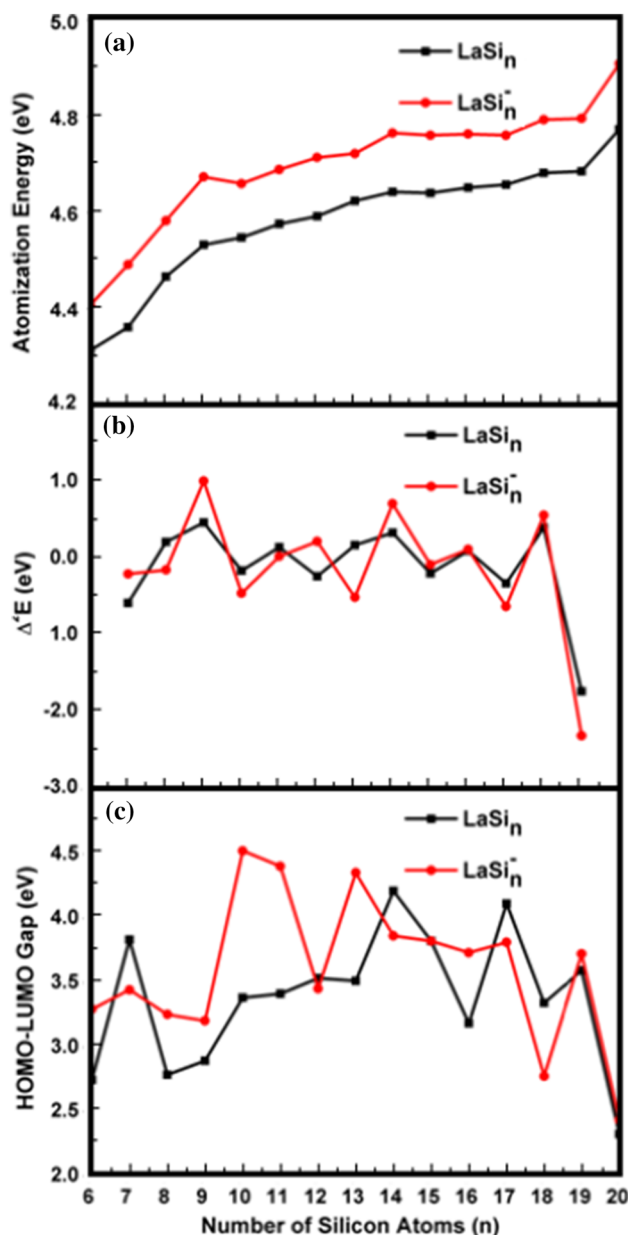To gain an in-depth understanding of the ideal thermodynamic stability and chemical reactivity of anionic $LaSi_{20}^-$

Fig. 4 Size dependences of **a** atomization energy (AE), **b** second energy difference (Δ^2E), and **c** HOMO–LUMO energy gap for the lowest energy $LaSi_n^-$ (n = 6–20) clusters

as mentioned above, the AdNDP method [51] is employed to perform quantitative insight into the nature of the bonding between the La atom and Si clusters. From Fig. 5 we can see that the chemical bonding of 84 valence electrons can be divided to two types: 2c–2e and 6c–2e. The Si_{20} outer fullerene cages are characterized by 30 2c–2e localized σ Si–Si bonds with 1.95 |e| in each bond. The 12 delocalized 6c–2e bonds with 1.96 |e| in each bond are responsible for the conjugation between the central La atom and the Si_{20} outer Fullerene shell and stabilize the encapsulated $LaSi_{20}^-$ species. In addition, the valence
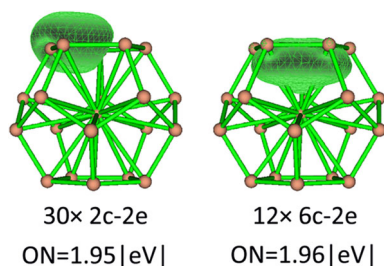
30× 2c-2e
ON=1.95|eV|

12× 6c-2e
ON=1.96|eV|

Fig. 5 AdNDP analysis of the $LaSi_{20}^{-}$ cluster. ON stands for the occupation number

electron filling of 84 magic number electrons for $LaSi_{20}^{-}$ is described as $1S^2 1P^6 1D^{10} 1F^{14} 1G^8 2S^2 1G^{10} 2P^6 2D^{10} 3S^2 2F^{14}$ in terms of spherical jellium model and the molecular orbital energies, which similar to that of superatom also stabilizes it.

Conclusions

The growth behavior and electronic properties of the lowest energy structures of neutral $LaSi_n$ ($n = 6$–20) and their anions have been explored by means of the ABCluster structure searching method combined with the mPW2PLYP double-hybrid density functional. The results revealed that the growth behavior of the lowest energy structures of anionic $LaSi_n^-$ ($n = 10$–20) clusters choose La-linked two silicon subclusters to La-encapsulated in silicon cages. For neutral $LaSi_n$ ($n = 6$–20), the growth behavior of the lowest energy structures from substitutional structure to linked motifs and finally to encapsulated configurations occurs at $n = 14$ and 20, respectively. The simulated photoelectron spectroscopy, adiabatic electron affinities, vertical detachment energies, relative stability and HOMO–LUMO energy gaps were presented. Analyses of HOMO–LUMO energy gaps, relative stability, and chemical bonding reveal that the $LaSi_{20}^-$ possesses faultless thermodynamic and chemical stability in a high I_h-symmetry endohedral motif, which can turn it into suitable constitutional units for cluster-assembled nanomaterials.

References

1. M. F. Jarrold (1991). *Science* **252**, 1085–1092.

2. E. C. Honea, A. Ogura, D. R. Peale, C. Félix, C. A. Murray, K. Raghavachari, W. O. Sprenger, M. F. Jarrold, and W. L. Brown (1999). *J. Chem. Phys.* **110**, 12161–12172.

3. I. Vasiliev, S. Öğüt, and J. R. Chelikowsky (1997). *Phys. Rev. Lett.* **78**, 4805–4808.

4. S. Nigam, C. Majumder, and S. K. Kulshreshtha (2006). *J. Chem. Phys.* **125**, 074303.

5. X. L. Zhu, X. C. Zeng, and Y. A. Lei (2004). *J. Chem. Phys.* **120**, 8985–8995.

6. J. C. Yang, W. G. Xu, and W. S. Xiao (2005). *J. Mol. Struct. Theochem.* **719**, 89–102.

7. L. P. Ding, F. H. Zhang, Y. S. Zhu, C. Lu, X. Y. Kuang, J. Lv, and P. Shao (2015). *Sci. Rep.* **5**, 15951.

8. W. G. Sun, J. J. Wang, C. Lu, X. X. Xia, X. Y. Kuang, and A. Hermann (2017). *Inorg. Chem.* **56**, 1241–1248.

9. Y. Y. Jin, Y. H. Tian, X. Y. Kuang, C. Z. Zhang, C. Lu, J. J. Wang, J. Lv, L. P. Ding, and M. Ju (2015). *J. Phys. Chem. A* **119**, 6738–6745.

10. Y. Y. Jin, G. Maroulis, X. Y. Kuang, L. P. Ding, C. Lu, J. J. Wang, J. Lv, C. Z. Zhang, and M. Ju (2015). *Phys. Chem. Chem. Phys.* **17**, 13590–13597.

11. X. D. Xing, A. Hermann, X. Y. Kuang, M. Ju, C. Lu, Y. Y. Jin, X. X. Xia, and G. Maroulis (2016). *Sci. Rep.* **6**, 19656.

12. B. L. Chen, W. G. Sun, X. Y. Kuang, C. Lu, X. X. Xia, H. X. Shi, and G. Maroulis (2018). *Inorg. Chem.* **57**, 343–350.

13. P. Shao, B. L. Chen, L. P. Ding, D. B. Luo, C. Lu, and X. Y. Kuang (2017). *Phys. Chem. Chem. Phys.* **19**, 25289–25297.

14. M. Ju, J. Lv, X. Y. Kuang, L. P. Ding, C. Lu, J. J. Wang, Y. Y. Jin, and G. Maroulis (2015). *RSC Adv.* **5**, 6560–6570.

15. L. P. Ding, P. Shao, C. Lu, F. H. Zhang, L. Ding, and T. L. Yuan (2016). *Phys. Chem. Chem. Phys.* **18**, 23296–23303.

16. M. Ohara, K. Koyasu, A. Nakajima, and K. Kaya (2003). *Chem. Phys. Lett.* **371**, 490–497.

17. K. Koyasu, J. Atobe, S. Furuse, and A. Nakajima (2008). *J. Chem. Phys.* **129**, 214301.

18. A. Grubisic, Y. J. Ko, H. P. Wang, and K. H. Bowen (2009). *J. Am. Chem. Soc.* **131**, 10783–10790.

19. A. J. Kenyon (2005). *Semicond. Sci. Technol.* **20**, R65–R84.

20. H. Tsunoyama, M. Shibuta, M. Nakaya, T. Eguchi, and A. Nakajima (2018). *Acc. Chem. Res.* **51**, 1735–1745.

21. X. X. Xia, A. Hermann, X. Y. Kuang, Y. Y. Jin, C. Lu, and X. D. Xing (2016). *J. Phys. Chem. C* **120**, 677–684.

22. R. N. Zhao, Y. H. Yuan, J. G. Han, and Y. H. Duan (2014). *RSC Adv.* **4**, 59331–59337.

23. R. N. Zhao and J. G. Han (2014). *RSC Adv.* **4**, 64410–64418.

24. T. G. Liu, W. Q. Zhang, and Y. L. Li (2014). *Front. Phys.* **9**, 210–218.

25. C. G. Li, L. J. Pan, P. Shao, L. P. Ding, H. T. Feng, D. B. Luo, and B. Liu (2015). *Theor. Chem. Acc.* **134**, 34.

26. J. C. Yang, J. Wang, and Y. R. Hao (2015). *Theor. Chem. Acc.* **134**, 81.

27. X. H. Xie, D. S. Hao, Y. M. Liu, and J. C. Yang (2015). *Comput. Theor. Chem.* **1074**, 1–8.

28. X. H. Xie, D. S. Hao, and J. C. Yang (2015). *Chem. Phys.* **461**, 11–19.

29. R. N. Zhao, R. Chen, Y. H. Yuan, F. Gu, and J. G. Han (2016). *J. Chem. Sci.* **128**, 365–371.

30. Z. Lenčéš, L. Benco, J. Madejová, Y. Zhou, L. Kipsová, and K. Hirao (2008). *J. Eur. Ceram. Soc.* **28**, 1917–1922.

31. H. Yu, L. L. Wang, J. L. Everaert, Y. L. Jiang, D. Mocuta, N. Horiguchi, N. Collaert, and K. D. Meyer (2017). *IEEE Electron Device Lett.* **38**, 843–846.

32. Q. Peng and J. Shen (2008). *J. Chem. Phys.* **128**, 084711.

33. T. T. Cao, X. J. Feng, L. X. Zhao, X. Liang, Y. M. Lei, and Y. H. Luo (2008). *Eur. Phys. J. D* **49**, 343–351.

34. D. B. Zhang and J. Shen (2004). *J. Chem. Phys.* **120**, 5104–5109.

35. Y. M. Liu, J. C. Yang, and L. Cheng (2018). *Inorg. Chem.* **57**, 12934–12940.
36. S. He and J. C. Yang (2017). *Theor. Chem. Acc.* **136**, 93.
37. H. M. Ning, Y. S. Gu, L. Cheng, and J. C. Yang (2018). *Chin. J. Struct. Chem.* **37**, 854–870.
38. J. C. Yang, Y. T. Feng, X. H. Xie, H. W. Wu, and Y. M. Liu (2016). *Theor. Chem. Acc.* **135**, 204.
39. Y. T. Feng, J. C. Yang, and Y. M. Liu (2016). *Theor. Chem. Acc.* **135**, 258.
40. L. Y. Hou, J. C. Yang, and Y. M. Liu (2017). *J. Mol. Model.* **23**, 117.
41. J. Zhang and M. Dolg (2015). *Phys. Chem. Chem. Phys.* **17**, 24173–24181.
42. J. P. Perdew, K. Burke, and M. Ernzerhof (1996). *Phys. Rev. Lett.* **77**, 3865–3868.
43. M. Dolg, H. Stoll, and H. Preuss (1993). *Theor. Chim. Acta.* **85**, 441–450.
44. M. Dolg, H. Stoll, A. Savin, and H. Preuss (1989). *Theor. Chim. Acta.* **75**, 173–194.
45. X. Y. Cao and M. Dolg (2001). *J. Chem. Phys.* **115**, 7348–7355.
46. D. E. Woon and T. H. D. Jr (1993). *J. Chem. Phys.* **98**, 1358–1371.
47. T. Schwabe and S. Grimme (2006). *Phys. Chem. Chem. Phys.* **8**, 4398–4401.
48. J. Akola, M. Manninen, H. Häkkinen, U. Landman, X. Li, and L. S. Wang (1999). *Phys. Rev. B* **60**, R11297.
49. D. J. Tozer and N. C. Handy (1998). *J. Chem. Phys.* **109**, 10180–10189.
50. T. Lu and F. W. Chen (2012). *J. Comput. Chem.* **33**, 580–592.
51. D. Y. Zubarev and A. I. Boldyrev (2008). *Phys. Chem. Chem. Phys.* **10**, 5207–5217.
52. M. J. Frisch, G. W. Trucks, H. B. Schlegel, G. E. Scuseria, M. A. Robb, J. R. Cheeseman, G. Scalmani, V. Barone, B. Mennucci, G. A. Petersson, H. Nakatsuji, M. Caricato, X. Li, H. P. Hratchian, A. F. Izmaylov, J. Bloino, G. Zheng, J. L. Sonnenberg, M. Hada, M. Ehara, K. Toyota, R. Fukuda, J. Hasegawa, M. Ishida, T. Nakajima, Y. Honda, O. Kitao, H. Nakai, T. Vreven, J. A. Montgomery Jr., J. E. Peralta, F. Ogliaro, M. Bearpark, J. J. Heyd, E. Brothers, K. N. Kudin, V. N. Staroverov, T. Keith, R. Kobayashi, J. Normand, K. Raghavachari, A. Rendell, J. C. Burant, S. S. Iyengar, J. Tomasi, M. Cossi, N. Rega, J. M. Millam, M. Klene, J. E. Knox, J. B. Cross, V. Bakken, C. Adamo, J. Jaramillo, R. Gomperts, R. E. Stratmann, O. Yazyev, A. J. Austin, R. Cammi, C. Pomelli, J. W. Ochterski, R. L. Martin, K. Morokuma, V. G. Zakrzewski, G. A. Voth, P. Salvador, J. J. Dannenberg, S. Dapprich, A. D. Daniels, O. Farkas, J. B. Foresman, J. V. Ortiz, J. Cioslowski, and D. J. Fox *Gaussian 09, Revision C.01* (Gaussian Inc, Wallingford, CT, 2010).
53. Q. Lu and K. A. Peterson (2016). *J. Chem. Phys.* **145**, 054111.
54. B. A. Hess (1985). *Phys. Rev. A* **32**, 756–763.
55. B. A. Hess (1986). *Phys. Rev. A* **33**, 3742–3748.
56. G. Jansen and B. A. Hess (1989). *Phys. Rev. A* **39**, 6016–6017.